Regulation of chromatin binding by a conformational switch in the tail of the Ran exchange factor RCC1

Yi Hao[1] and Ian G. Macara[2]

[1]Department of Cell Biology and [2]Department of Microbiology, Center for Cell Signaling, University of Virginia, Charlottesville, VA 22908

RCC1 is the only known exchange factor for the Ran guanosine triphosphatase and performs essential roles in nuclear transport, spindle organization, and nuclear envelope formation. RCC1 binds to chromatin through a bimodal attachment to DNA and histones, and defects in binding cause chromosome missegregation. Chromatin binding is enhanced by apo-Ran. However, the mechanism underlying this regulation has been unclear. We now demonstrate that the N-terminal tail of RCC1 is essential for association with DNA but inhibits histone binding. Apo-Ran significantly promotes RCC1 binding to both DNA and histones, and these effects are tail mediated. Using a fluorescence resonance energy transfer biosensor, we detect conformational changes in the tail of RCC1 coupled to the two binding modes and in response to interactions with Ran and importin-α. The biosensor also reports changes accompanying mitosis in living cells. We propose that Ran induces an allosteric conformational switch in the tail that exposes the histone-binding surface on RCC1 and facilitates association of the positively charged tail with DNA.

Introduction

The Ran GTPase performs vital functions throughout the eukaryotic cell cycle. During interphase, high RanGTP within the nucleus drives the vectorial transport of cargo between the nuclear and cytoplasmic compartments (Terry et al., 2007; Trinkle-Mulcahy and Lamond, 2007; Yoon et al., 2008). In organisms with open mitoses, RanGTP stabilizes spindle microtubules near chromatin and facilitates kinetochore attachment (Carazo-Salas et al., 1999; Kalab et al., 1999; Zhang et al., 1999; Gruss et al., 2001; Gruss and Vernos, 2004; Silverman-Gavrila and Wilde, 2006), whereas in telophase, RanGTP is required for reassembly of the nuclear envelope (Zhang and Clarke, 2000; Walther et al., 2003). These functions depend on association of the Ran guanine nucleotide exchange factor with chromatin, which spatially restricts the generation of RanGTP (Kalab et al., 2002, 2006; Caudron et al., 2005).

In vertebrates, the Ran guanine nucleotide exchange factor is called RCC1 (Bischoff and Ponstingl, 1991). RCC1 resembles a donut, from which protrudes a flexible N-terminal tail consisting of aa 1–20 (Renault et al., 1998). Early studies suggested that the tail binds DNA (Seino et al., 1992; Chen et al., 2007), and recently we demonstrated that this association is facilitated by an unusual posttranslational modification of RCC1 in which the initial Met residue is removed and the exposed α-amino group (Ser in primates and Pro in other vertebrates) is tri- or dimethylated (Chen et al., 2007). Deletion of the tail or mutations of RCC1 that block methylation show weaker binding to chromatin, which causes mitotic defects (Moore et al., 2002; Chen et al., 2007). However, the isolated N terminus binds only weakly to chromatin (Chen et al., 2007). A second important binding mode occurs through histones H2A/H2B (Nemergut et al., 2001).

The RCC1 tail is a locus for multiple regulatory mechanisms. It contains an NLS, which is recognized by the transport factor importin-α3 (Impα3; Nemergut and Macara, 2000; Talcott and Moore, 2000; Moore et al., 2002), and Impα binding can interfere with chromatin association. Mitotic phosphorylation of the tail has been reported to block Impα3 binding, thereby stabilizing chromatin association (Hutchins et al., 2004; Li and Zheng, 2004). In addition, there are three splice variants of RCC1,

Correspondence to Ian G. Macara: igm9c@virginia.edu

Abbreviations used in this paper: FRET, fluorescence resonance energy transfer; Imp, importin; WT, wild type.

The online version of this article contains supplemental material.

The Rockefeller University Press $30.00
J. Cell Biol. Vol. 182 No. 5 827–836
www.jcb.org/cgi/doi/10.1083/jcb.200803110

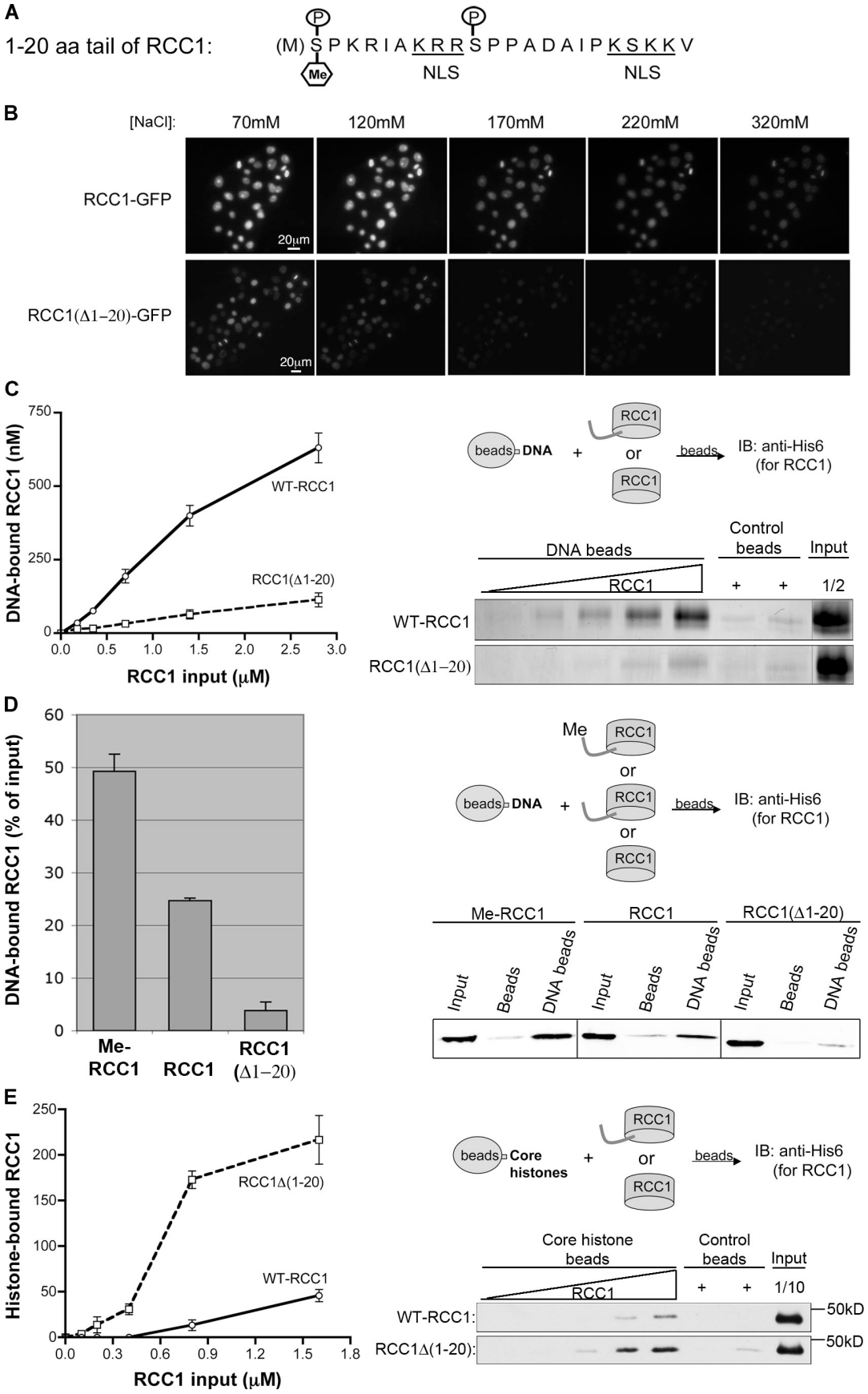

Figure 1. **The N-terminal tail controls binding to both DNA and histones.** (A) Amino acid sequence of the human RCC1 N-terminal tail. (B) Deletion of the tail significantly decreases chromatin binding. MDCK cells plated on a poly-lysine–coated coverglass were permeabilized, and identical concentrations of recombinant proteins RCC1-YFP and RCC1(Δ1–20)-YFP were added. Images were collected before and after the cells were washed sequentially with buffers

α, β, and γ, and the β and γ variants contain unique inserts downstream of the tail, which affect chromatin binding (Hood and Clarke, 2007).

RCC1 association with chromatin is also regulated by Ran. The dynamic interaction of RCC1 with chromatin in living cells is stabilized by Ran(T24N), a mutant that mimics the apo state of the GTPase and forms a stable binary complex with RCC1 (Li and Zheng, 2004). Conversely, a mutation in RCC1 (D182A) that disrupts Ran binding destabilizes chromatin association (Moore et al., 2002; Hutchins, et al., 2004). Mutational analyses have suggested that one face of the RCC1 donut binds to chromatin (Seino et al., 1992), whereas the other face binds Ran (Renault et al., 2001). In this study, we address the question of how Ran on one side of RCC1 can regulate chromatin binding to the other. We propose that the tail undergoes an allosteric conformational change upon binding Ran. In the closed state, the tail inhibits histone binding, whereas in the open state, the tail permits histone binding and can more readily bind DNA.

Results and discussion

How does Ran enhance the binding of its exchange factor, RCC1, to chromatin? Steric effects are unlikely because Ran binds to one face of RCC1 and chromatin to the opposite face. An alternative mechanism involves allosteric switching, but the crystal structures of RCC1 alone and Ran(T24N)-bound RCC1 are almost identical to one another. However, the 20-aa N-terminal tail is absent from both structures and is assumed to be flexible (Renault et al., 1998, 2001). Therefore, we reasoned that Ran binding might cause a conformational change in the tail. To test this hypothesis, we needed to know whether the first 20 aa are necessary for chromatin binding. Deletion of aa 1–27 results in a diffusive cytoplasmic distribution of RCC1 (Moore et al., 2002), but this deletion also removes residues that lie across the chromatin-binding face of the RCC1 donut and interact with key amino acids on this surface.

Because the NLS lies within the first 20 aa (Fig. 1 A), we used cells permeabilized with Triton X-100 to remove the nuclear envelope and added recombinant YFP-tagged wild-type (WT) RCC1 α isoform or RCC1(Δ1–20) proteins. Using recombinant proteins also avoids the complication of α-N-methylation. The cells were washed with increasing salt concentrations, and retained YFP-RCC1 was imaged (Fig. 1 B). RCC1(Δ1–20) showed substantially reduced binding to chromatin as compared with WT-RCC1, even at the lowest salt concentration (70 mM), and was almost entirely lost at higher concentrations, whereas WT-RCC1 was partially retained by chromatin even at 320 mM NaCl, suggesting that the 1–20-aa tail is essential for stable chromatin binding.

The RCC1 tail is believed to bind DNA, probably by electrostatic interactions between positively charged amino acids (Fig. 1 A) and the negatively charged DNA (Seino et al., 1992). Therefore, we next assayed the binding of His6-tagged WT-RCC1 and RCC1(Δ1–20) to DNA beads and to core histone octamers coupled to beads. Bound RCC1 was detected by immunoblotting with anti-His6 antibody. Under salt concentrations close to physiological, deletion of the N-terminal tail drastically reduced the binding of RCC1 to DNA beads compared with WT-RCC1, confirming that the tail is necessary for DNA binding (Fig. 1 C). Next, because the N-terminal α-amino group of RCC1 is methylated in mammalian cells, the DNA binding capacities of in vitro methylated RCC1, recombinant RCC1, and RCC1(Δ1–20) were also compared. Confirming our previous study (Chen et al., 2007), methylation of RCC1 resulted in elevated binding to DNA (Fig. 1 D).

The region of RCC1 that interacts with histones has not been previously established. Surprisingly, deletion of the tail strongly increased binding to core histone-conjugated beads (Fig. 1 E). This result suggests that the tail inhibits RCC1 binding to histones either by charge repulsion or by screening the interaction surface. In either case, one can imagine that a conformational change in the tail might modulate the ability of RCC1 to bind chromatin. To detect such conformational switches, we developed a fluorescence resonance energy transfer (FRET)–based RCC1 biosensor. Because both the N and C termini of RCC1 extend from the same side of the donut, we predicted that a FRET pair attached to the ends would be sufficiently close to interact. CFP was fused to the N terminus, and YFP was fused to the C terminus of RCC1 (Fig. 2 A). The CFP-RCC1-YFP fusion was expressed in HEK293T cells, and emission spectra were collected from the soluble fraction. Lysates from cells expressing CFP alone and YFP alone were also analyzed. The CFP-RCC1-YFP emission spectrum showed a large peak at 522 nm, corresponding to YFP emission, which demonstrates that, as expected, the biosensor exhibits efficient FRET (Fig. 2 B).

We next asked whether this biosensor could be used to detect conformational changes in RCC1. Impα3 binds to an NLS in the tail, and because it is a large (50 kD) protein, it might be expected to force the tail away from the body of RCC1, which could change either the distance or orientation between fluorophore dipoles of the biosensor. Therefore, we tested whether the biosensor would detect this interaction. In the presence of Impα3, FRET efficiency of CFP-RCC1-YFP showed a saturable decrease (Fig. 2, C and D), which is consistent with the known affinity of Impα for monopartite NLSs (Nemergut and Macara, 2000). This result demonstrates that the biosensor is sensitive to direct interactions with the N-terminal tail.

To test whether DNA binding to the tail would also alter its conformation, we added increasing concentrations of annealed

containing indicated NaCl concentrations. (C) Deletion of the tail abolishes DNA binding. Recombinant RCC1-His_6 or RCC1(Δ1–20)-His_6 proteins were incubated with DNA-agarose beads or plain agarose beads. Bound proteins were detected by Coomassie blue staining. The gels were scanned and quantified by densitometry (left). The right panel shows representative DNA binding. (D) α-N-amino methylation of RCC1 further promotes RCC1 binding to DNA. Recombinant RCC1(Δ1–20)-His_6, WT RCC1-His_6, or purified Me-RCC1-His_6, which had been methylated in vitro, was incubated with agarose beads as in B. Proteins were detected and quantified by immunoblotting with anti-His6 antibody and an Odyssey scanner. (E) The RCC1 tail negatively regulates histone binding. Recombinant RCC1-His_6 or RCC1(Δ1–20)-His_6 was incubated at various concentrations with biotin-labeled core histones on streptavidin beads or with streptavidin beads alone. Bound proteins were detected by ECL with anti-His6 antibody (right) and quantified (left) as in B. Error bars represent ±1 SD.

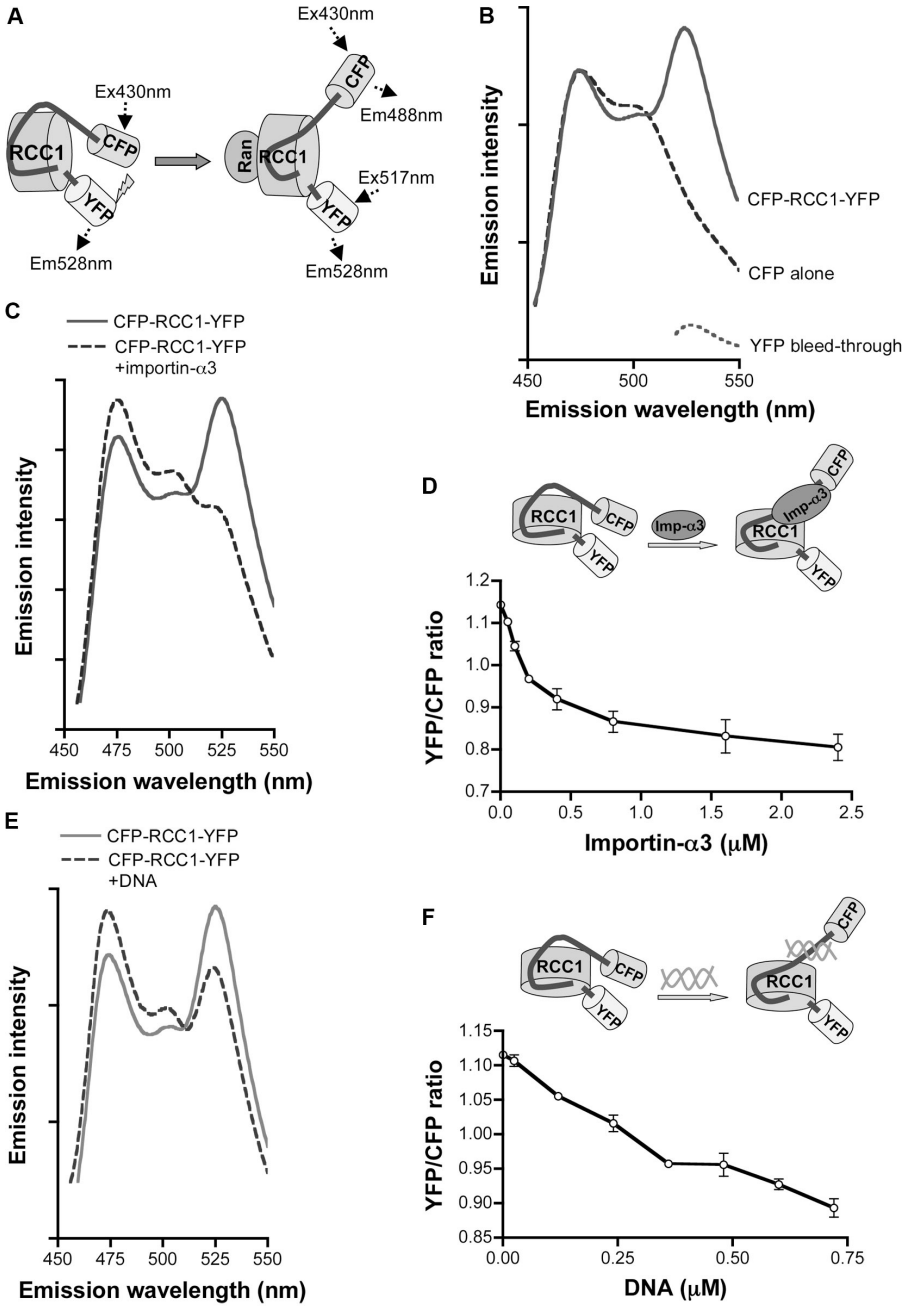

Figure 2. **Development of FRET-based RCC1 biosensor.** (A) Schematic of the FRET-based RCC1 biosensor CFP-RCC1-YFP. (B) The biosensor CFP-RCC1-YFP exhibits efficient FRET. Excitation was at 430 nm. Emission spectra are shown for CFP alone, YFP alone, and for CFP-RCC1-YFP. (C) FRET efficiency of CFP-RCC1-YFP is saturably reduced by Impα3; representative emission spectra ± Impα3. (D) Titration of the emission ratio (YFP/CFP) versus increasing concentrations of Impα3. (E) DNA decreases FRET efficiency of CFP-RCC1-YFP in a dose-dependent manner. Annealed 64-nt complimentary oligonucleotides were used as the source of DNA. FRET efficiencies were measured in the presence of increasing concentrations of oligonucleotides. Emission spectrum is shown ± DNA. (F) Titration of emission ratio (YFP/CFP) versus increasing DNA concentration. For D and F, error bars represent ±1 SD.

64-mer oligonucleotides and observed a dose-dependent decrease in FRET efficiency (Fig. 2, E and F). Note that the CFP emission increases as the YFP emission drops, confirming that the response resulted from a change in FRET efficiency rather than collisional quenching or other nonspecific effects. Moreover, because the biosensor cannot be α-amino methylated, it tests conformational changes independently of α-methylation–mediated effects on DNA binding (Chen et al., 2007). We conclude that the biosensor can detect changes in the conformation of the RCC1 tail and that both Impα3 and DNA can alter this conformation.

Ran binds to the face of RCC1 opposite to that from which the N and C termini protrude. Moreover, Ran binding does not alter the structure of the body of the RCC1 protein (Renault et al., 1998, 2001). A priori, therefore, one would not expect Ran binding to change the orientation or position of the N-terminal tail. However, the FRET efficiency of the biosensor was significantly reduced in a saturable manner by the addition of Ran(T24N) (Fig. 3, A and B), whereas the addition of BSA as a negative control did not affect FRET (not depicted). To exclude the possibility that the FRET reduction might be caused by interference from other proteins in cell lysate, we purified a recombinant biosensor from *Escherichia coli,* His_6-CFP-RCC1-YFP-Flag. This fusion protein exhibits the same emission characteristics as the protein expressed in HEK293T cells and gave a similar response upon addition of Ran(T24N) (Fig. S1 A, available at http://www.jcb.org/cgi/content/full/jcb.200803110/DC1). These data identify an allosteric response of the N-terminal tail of RCC1 to Ran binding.

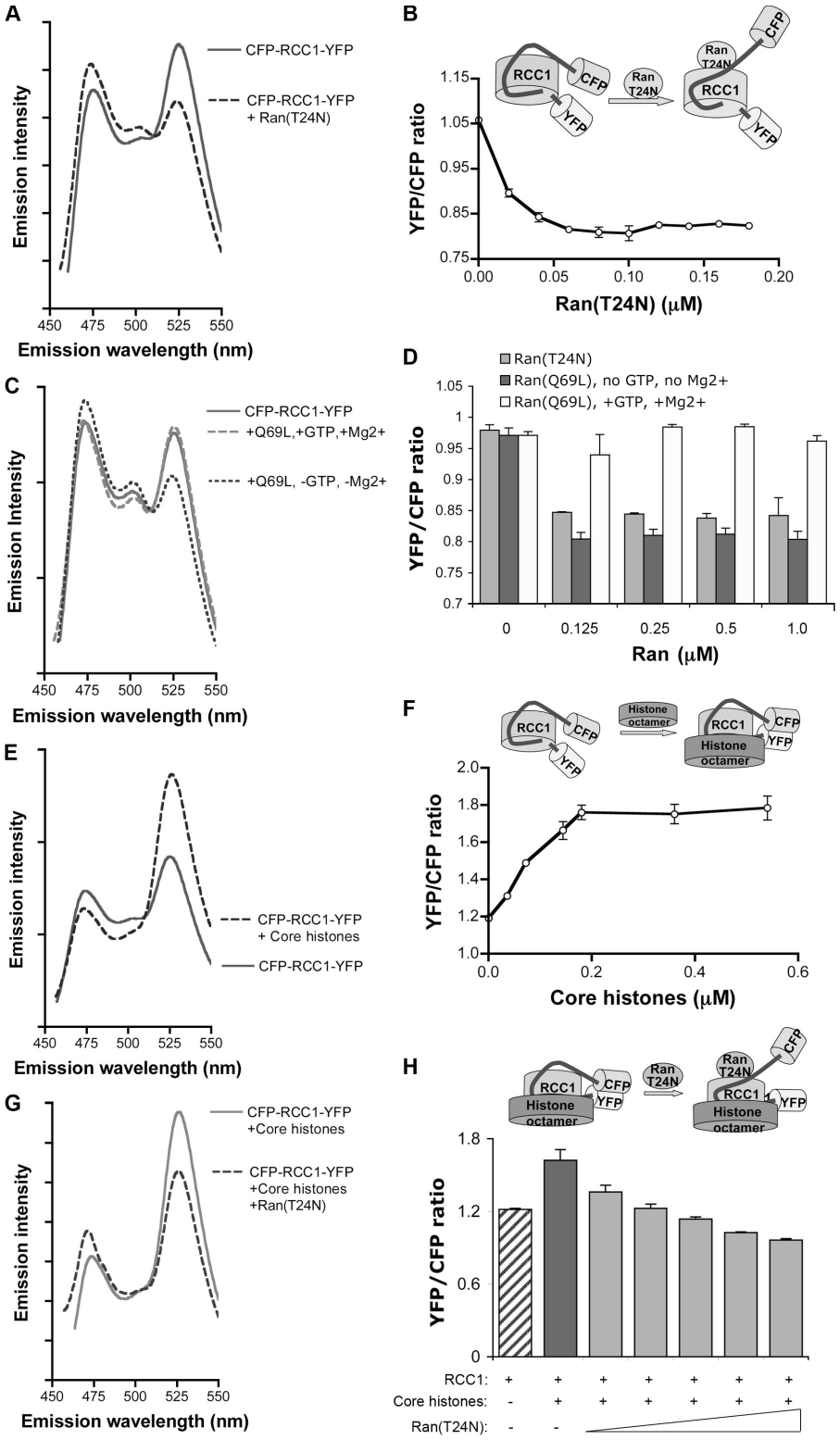

Figure 3. **Ran(T24N) binding triggers a conformational switch in the RCC1 tail.** (A) Ran(T24N) decreases FRET efficiency of the RCC1 biosensor. Emission spectra are shown ± recombinant Ran(T24N), with excitation at 430 nm. (B) Titration of FRET efficiency with increasing Ran(T24N) concentration. (C) GTP-bound Ran(Q69L) does not change FRET efficiency. Emission spectra were obtained ± recombinant Ran(Q69L) and ± GTP and Mg^{2+}. (D) Quantification of YFP/CFP emission ratio at different concentrations of Ran(Q69L) in the presence or absence of GTP and Mg^{2+}. Emission efficiencies are compared with those in the presence of equivalent concentrations of Ran(T24N). (E) Core histones increase FRET efficiency. Emission spectra are shown ± purified core histone octamer. (F) Titration of YFP/CFP emission ratio with increasing concentrations of core histones. (G) Ran(T24N) can still decrease FRET efficiency even in the presence of histones. Recombinant Ran(T24N) was added after the addition of histones. (H) Quantification of emission ratios (YFP/CFP) when titrating with Ran(T24N) in the presence of histones. Error bars represent ±1 SD.

The T24N mutant does not efficiently bind guanine nucleotides and so mimics the apo-Ran transition state in the nucleotide exchange reaction. For this reason, it binds RCC1 with an affinity ~10-fold higher than that of GDP- or GTP-bound Ran (Klebe et al., 1995). Therefore, to further confirm that the Ran(T24N)-induced FRET decrease was caused by binding of Ran to the RCC1, emission spectra were measured in the presence of Ran(Q69L), a Ran mutant deficient in nucleotide hydrolysis that binds to RCC1 weakly. In the absence of GTP and Mg^{2+}, Ran(Q69L) behaved like Ran(T24N), decreasing the FRET efficiency of the biosensor (Fig. 3, C and D). However, in the presence of GTP and Mg^{2+}, Ran(Q69L) did not change the FRET efficiency, even at high concentrations (Fig. 3, C and D). These results confirm that the effect of Ran(T24N) is mediated by its binding to RCC1.

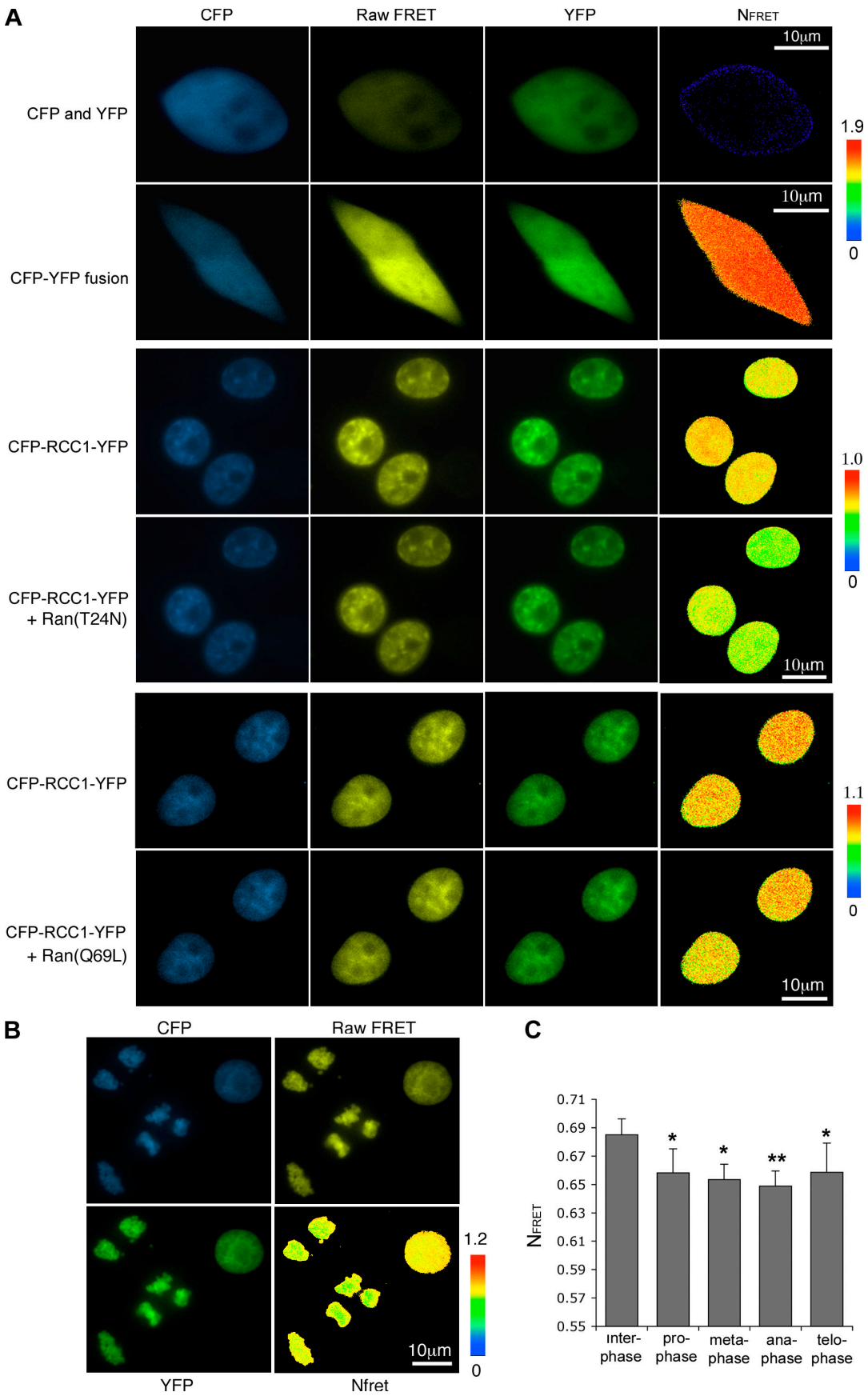

Figure 4. **FRET imaging reveals conformational changes in RCC1 bound to chromatin upon binding Ran(T24N) and during mitosis in MDCK cells.** (A) Ran(T24N) binding reduces FRET efficiency of the CFP-RCC1-YFP biosensor bound to chromatin. Cotransfection of CFP and YFP was used as a negative control for FRET (top), and CFP-YFP fusion was used as a positive control (middle). After permeabilization with 0.1% Triton X-100, cells were imaged ± recombinant

Because Ran binds to one side of the RCC1 body and chromatin is believed to bind to the other, we were also interested in whether histones would perturb the conformational alteration in the tail. Surprisingly, addition of core histones caused a significant increase in the FRET efficiency (Fig. 3 E). This change was saturable with increasing histone concentration (Fig. 3 F). Because the C and N termini are on the same chromatin-binding face, core histones might push the two termini closer together, resulting in elevated FRET. When Ran(T24N) was added together with histones, FRET efficiency could still be reduced by Ran(T24N) (Fig. 3 G). At high concentrations, Ran(T24N) completely overrode the FRET increase induced by core histones, suggesting that core histones and Ran(T24N) have independent effects on conformation of the RCC1 tail (Fig. 3 H).

Does a Ran(T24N)-triggered conformational change also occur when RCC1 is associated with intact chromatin? To address this issue, the biosensor was expressed in MDCK cells. The cells were permeabilized and imaged by FRET microscopy before and after the addition of Ran(T24N). Raw FRET images were corrected for donor bleedthrough, acceptor bleedthrough, and for levels of both donor and acceptor to acquire normalized FRET (N_{FRET}) images. Cells cotransfected with CFP and YFP as a negative control showed no detectable FRET signal, whereas cells expressing a CFP-YFP fusion protein as a positive control generated a high FRET signal as expected. CFP-RCC1-YFP gave a signal lower than that of the CFP-YFP fusion. When recombinant Ran(T24N) was added, N_{FRET} was significantly reduced (Fig. 4 A). As expected, however, addition of Ran(Q69L) had no effect (Fig. 4 A). To rule out the possibility that permeabilization might affect the dynamics of the RCC1 binding to chromatin, we also transiently cotransfected the biosensor together with Ran(T24N) and measured FRET efficiency in live cells (Fig. S1 B). N_{FRET} was consistently reduced by the presence of the Ran mutant.

RCC1-chromatin dynamics are somewhat faster in mitosis than interphase (Li et al., 2003; Hutchins et al., 2004). Using our biosensor, we found that mitotic cells display a slight but consistent reduction in FRET as compared with interphase cells, with the FRET efficiency dropping through anaphase and going up at the end of mitosis (Fig. 4, B and C). Thus, conformational changes might contribute to the different dynamics of RCC1-chromatin association during progression through mitosis. Together, these results demonstrate that apo-Ran binding triggers a conformational switch in the tail of RCC1, even when the protein is bound to chromatin. Small conformational alterations also occur in mitosis.

What is the function of this conformational change? To determine whether and how the Ran-induced conformational change in the tail might regulate chromatin association, we conducted in vitro binding assays using DNA- and histone-conjugated beads. Binding of RCC1-His_6 was compared ± a molar excess of Ran(T24N). RCC1 binding to DNA was substantially increased by Ran(T24N), suggesting that the conformational change makes the tail more accessible to DNA (Fig. 5 A). Intriguingly, Ran(T24N) also promoted the interaction of RCC1 with histones (Fig. 5 B). This result is consistent with the aforementioned data that the tail inhibits histone binding and with the idea that a Ran-induced conformational switch releases the inhibition. To test this model more decisively, we measured the binding of tailless RCC1 to histones in the presence or absence of Ran(T24N). As shown in Fig. 5 C, the affinity of RCC1(Δ1–20) for histones was constitutively high and was not further increased by the Ran mutant. We conclude that the effects of Ran(T24N) are mediated by a conformational switch in the N-terminal tail.

We note that Ran can also bind directly to chromatin through histones H3/H4 (Bilbao-Cortés et al., 2002). However, the Ran(T24N) mutant does not appear able to bind histones (Bilbao-Cortés et al., 2002), so it is unlikely to influence RCC1-chromatin association through this mechanism.

Mitotic phosphorylation of the tail has been reported to prevent RCC1 association with Impα3, thereby stabilizing chromatin binding (Hutchins et al., 2004; Li and Zheng, 2004). Consistent with this, the addition of Impα3 reduced the association of our biosensor with chromatin in permeabilized cells (Fig. S2 A, available at http://www.jcb.org/cgi/content/full/jcb.200803110/DC1), indicating that Impα3 could potentially block chromatin binding of RCC1 by associating with its NLS. However, it is unlikely that the Imp blocks RCC1 binding in intact cells because high RanGTP concentrations near the chromatin surface would prevent the Impα/β complex from associating with NLSs and would also promote association of Impα with its export factor, CAS. To determine the molecular mechanism by which Impα regulates RCC1 binding to chromatin, we examined RCC1 retention on DNA beads and histone beads ± Impα3. As expected, the addition of Impα3 significantly reduced RCC1 binding to DNA, possibly by directly blocking the DNA-binding region or pulling the tail away (Fig. S2 B). Strikingly, however, the addition of Impα3 increased RCC1 binding to core histones (Fig. 5 C), which is consistent with the effects of deletion of the tail on core histone binding and further supports the idea that conformational changes in the tail can relieve its inhibitory effect on histone association. These data are summarized in Table S1 (available at http://www.jcb.org/cgi/content/full/jcb.200803110/DC1).

We conclude that RCC1 binding to chromatin can be regulated by an allosteric switch mechanism (Fig. 5 E). The RCC1 tail binds to DNA, whereas its body interacts with histones H2A/H2B. The tail can also inhibit association with histones. It undergoes a conformational switch in response to Ran binding, DNA binding, or to interactions with Impα3. We propose that in its closed state, RCC1 has a low affinity for both DNA and histones. Ran binding causes the tail to swing away from the body,

Ran(T24N) (middle) or Ran(Q69L) (bottom). After subtracting background, raw FRET images were corrected for donor and acceptor bleedthrough and for expression levels of donor and acceptor to obtain N_{FRET} images. (B) FRET efficiency is slightly but consistently reduced in mitotic cells. FRET imaging was performed on live cells expressing the RCC1 biosensor. Representative N_{FRET} images of interphase cells and anaphase cells. (C) Quantification of N_{FRET} efficiencies in interphase, prophase, metaphase, anaphase, and telophase cells. N_{FRET} intensities of 61 cells at different phases were measured, and the mean N_{FRET} values are compared. Error bars represent ±SD. *, $P < 0.05$; **, $P < 0.001$.

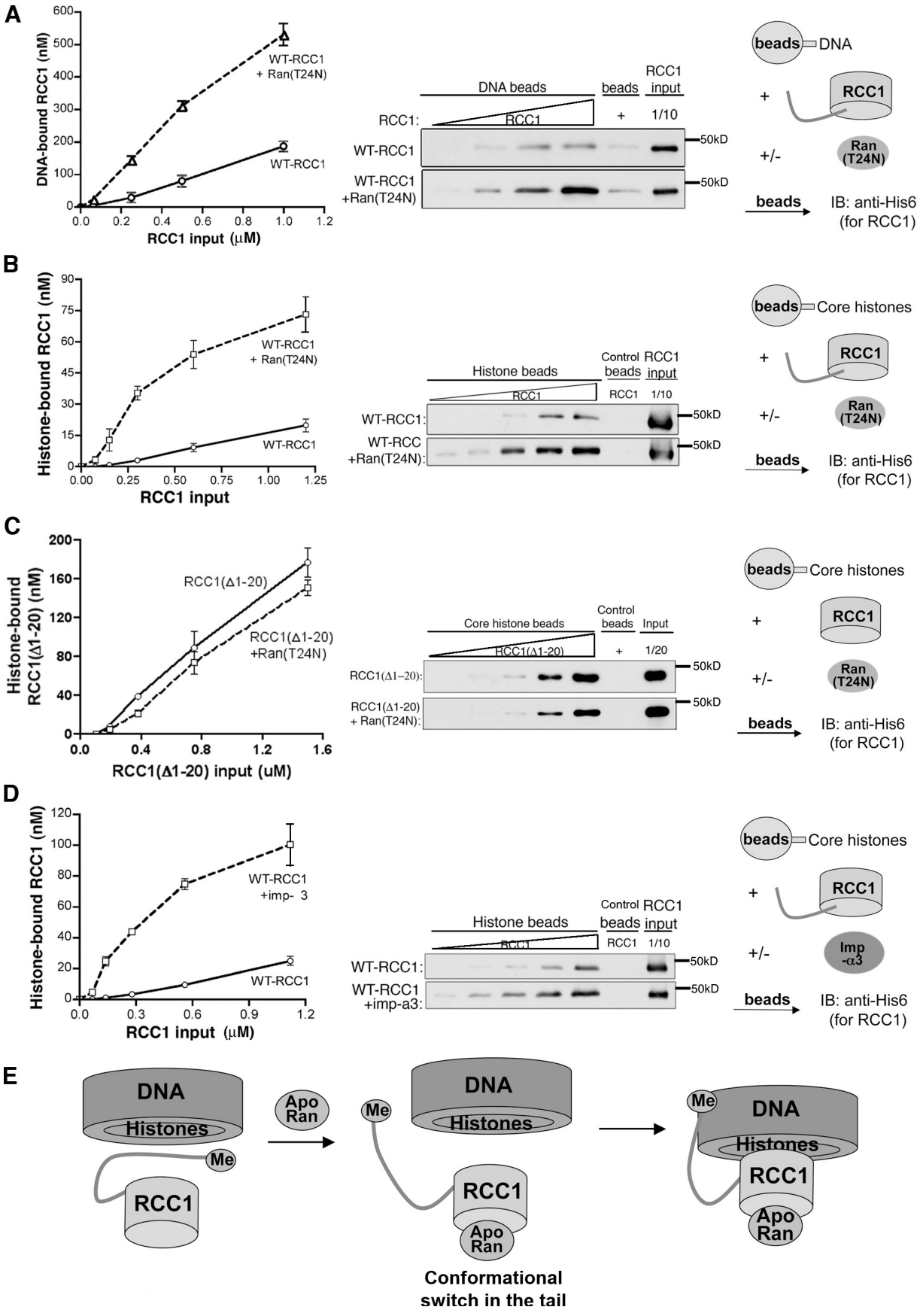

Figure 5. **Ran(T24N) promotes both RCC1 bindings to DNA and histones in vitro.** The effects of Ran(T24N) require the RCC1 tail. (A) RCC1 binding to DNA is promoted by Ran(T24N). (B) RCC1 binding to core histones is increased by Ran(T24N). (C) Ran(T24N) has no effect on RCC1(Δ1–20) binding to core histones. (D) Core histone binding of RCC1 is increased by Impα3. (E) Conformational switch model. The N-terminal tail of RCC1 is essential for DNA

exposing the histone-binding surface and enabling the positively charged tail to interact efficiently with DNA. Moreover, this bimodal binding mechanism is enhanced by α-N-methylation. Other factors, such as RanBP3, might also play important roles in regulating RCC1 conformation and chromatin association (Nemergut et al., 2002; Yoon et al., 2008). Together, such factors likely control the RanGTP gradient around chromatin and are essential for ensuring normal chromosome segregation, nuclear envelope formation, and nucleocytoplasmic transport.

Materials and methods

Constructs

To generate RCC1-His_6, RCC1(Δ1–20)-His_6, RCC1-YFP-His_6, and RCC1(Δ1–20)-YFP-His_6, human RCC1 or RCC1-YFP was amplified to introduce a 5′ NdeI site and 3′ XhoI site and was subcloned into pET-30a (Novagen). To enable purification of full-length CFP-RCC1-YFP, His_6 was added to the N terminus, and a Flag tag was added at the C terminus. A 5′ BamHI site and a 3′ NotI site were introduced into RCC1, and they were subcloned into pTAC-His_6-CFP-YFP to produce pTAC-His_6-CFP-RCC1-YFP. RCC1-YFP was then amplified to introduce a 5′ NotI site, a C-terminal Flag tag, and a 3′ XbaI site, and this replaced the original RCC1-YFP to generate pTAC-His_6-CFP-RCC1-YFP-Flag. To make CFP-RCC1-YFP for expression in mammalian cells, RCC1 was amplified to introduce a 5′ BamHI site and a 3′ NotI site and was subcloned into pK-seFRET.

Protein expression and purification

PET-30a or pTAC constructs were transformed into BL21(DE3) or XLI-blue. Bacterial cells were cultured at 37°C until OD_{600} = ∼0.8. IPTG was then added to 500 µM for pET-30a constructs or 200 µM for pTAC constructs, and the cultures were incubated overnight at 18°C. Cells were collected by centrifugation and resuspended in buffer containing 20 mM Hepes-KOH, pH 7.9, 500 mM NaCl, 1 mM $MgCl_2$, and 10% glycerol supplemented with 1 mM PMSF plus 5 µg/ml aprotinin, 5 µg/ml leupeptin, and 5 µg/ml pepstatin. Cells were broken using a French press. All His_6-tagged proteins were purified using Ni–nitrilotriacetic acid beads (QIAGEN). His6-CFP-RCC1-YFP-Flag was further purified using M2-agarose beads (Sigma-Aldrich) to generate full-length recombinant protein. Core histones were purified from chicken red blood cells as described previously (Lutter, 1978; Simon and Felsenfeld, 1979; Sandeen et al., 1980).

In vitro methylation of RCC1

HeLa nuclear extract was prepared as described previously (Dignani et al., 1983). In vitro methylation was performed at 30°C for 2.5 h in a 200-µl reaction containing 16 µg recombinant RCC1, 200 µg HeLa nuclear extract, and 150 µM SAM (*S*-adenosyl-L-methy-methionine; Sigma-Aldrich) in methylation buffer containing 50 mM Tris-HCl, pH 8.0, 1 mM PMSF, and 25 mM NaCl. The methylated RCC1 protein was then repurified using Ni–nitrilotriacetic acid beads as described in the previous section.

Cell culture and transfection

HEK293T cells were cultured in DME supplemented with 5% calf serum, 5% FBS, 100 Uml^{-1} penicillin, and 100 Uml^{-1} streptomycin (Invitrogen). MDCK cells were cultured in DME supplemented with 5% FBS, 100 Uml^{-1} penicillin, and 100 Uml^{-1} streptomycin. HEK293T cells were transfected by calcium phosphate. For MDCK cells, plasmids were introduced by nucleofection (Amaxa). 2 µg DNA was used in each transfection for 2 × 10^6 cells. Transfection efficiency was generally >70%.

Chromatin-binding assay

MDCK cells growing on poly-lysine–coated coverglass chambers were permeabilized with 0.1% Triton X-100 for 5 min at 23°C. Proteins were added to a final concentration of 4 µM in buffer containing 10 mM $NaPO_4$, pH 7.2, 70 mM KCl, 250 mM sucrose, and 1 mM $MgCl_2$ and incubated for 10 min at 23°C. Cells were rinsed with the same buffer and imaged using an inverted microscope (Axiovert; Carl Zeiss, Inc.) with a 40× NA 0.9 Plan-Neofluar lens coupled to a charge-coupled device camera (Orca; Hamamatsu). Images were collected at 12-bit depth and 1,024 × 1,280–pixel resolution using Openlab 5.0 software (Improvision). The cells were imaged sequentially after washing with buffers containing 120 mM, 170 mM, 220 mM, and 320 mM NaCl. Images were finally converted to 8-bit TIFF files and compiled using Photoshop 7.0 (Adobe).

In vitro binding assays

DNA-conjugated agarose beads were purchased from GE Healthcare. Purified core histones were biotin labeled with sulfosuccinimidyl-2-[biotinamido]ethyl-1,3-dithiopropionate biotin (Thermo Fisher Scientific) and conjugated to streptavidin beads (Thermo Fisher Scientific)). DNA-binding assays were performed in buffer containing 25 mM Hepes, pH 7.2, 150 mM NaCl, 2 mM $MgCl_2$, 1 mM DTT, and 25% glycerol. Histone in vitro binding assays were performed in 20 mM MOPS, pH 7.1, 150 mM NaCl, 5 mM Mg-acetate, and 0.1% NP-40. Binding reactions were incubated at 4°C for 30 min. Beads were washed four times, and bound proteins were detected by Coomassie blue staining or by immunoblotting with mouse monoclonal anti-His_6 antibody (Covance) and either chemiluminescence (ECL) or with an Odyssey system (Li-Cor). To quantify ECL and Coomassie band intensities, gels or blots were scanned, and the TIFF files were analyzed using ImageJ (National Institutes of Health [NIH]).

FRET spectroscopy

CFP-RCC1-YFP was expressed in HEK293T cells as described in Cell culture and transfection. After 24–48 h, cell lysates were prepared in 25 mM Hepes, pH 7.5, 10 mM $MgSO_4$, 500 mM NaCl, and 0.5% Triton X-100 supplemented with 2 mM DTT, 1 mM PMSF, 10 µg/ml leupeptin, and 20 µg/ml aprotinin. Proteins were diluted in buffer containing 25 mM Hepes, pH 7.5, and 2 mM $MgSO_4$. Samples were excited at 430 nm (slit width of 4 nm), and emission spectra were collected between 450 and 550 nm (slit width of 4 nm) on a Fluorolog-3 spectrofluorometer (FL3-11tau; Jobin Yvon, Inc.) using a 5-mm rectangular quartz cuvette at 25°C. FRET efficiency changes were calculated as the ratio of the emission intensity peak of YFP to the emission intensity peak of CFP.

FRET microscopy

To determine donor and acceptor bleedthrough correction factors, CFP and YFP were transfected separately into MDCK cells, and images were obtained in the CFP, YFP, and FRET channels (CFP excitation/YFP emission) using an inverted microscope (Eclipse T200; Nikon) with a 60× NA 1.2 Plan Achromatic water immersion lens and Orca camera set at 1 × 1 binning. Openlab 5.0 software was used for acquisition. Excitation intensity was attenuated with a 75% neutral density filter to prevent photobleaching. Exposure times were ∼300 ms. Excitation and emission filters were as follows: CFP excitation (S436/10×) and emission (S470/30 m) and YFP excitation (S500/20×) and emission (S535/30 m; Chroma Technology Corp.). For each FRET experiment, CFP, YFP, and FRET images were collected under identical conditions. After subtracting background, raw FRET images were corrected for bleedthrough and normalized for both donor level and acceptor level to obtain N_{FRET} using the Openlab FRET module (Improvision). Images were compiled using Photoshop 7.0.

Online supplemental material

Fig. S1 shows that Ran(T24N) decreases the FRET efficiency in vitro and in vivo. Fig. S2 shows that Impα3 significantly decreases chromatin binding and DNA binding of RCC1 in permeabilized MDCK cells. Table S1 shows the summary of FRET and in vitro DNA/histone binding data. Online supplemental material is available at http://www.jcb.org/cgi/content/full/jcb.200803110/DC1.

We thank members of the Macara laboratory for helpful discussions. We also thank L. Pemberton for core histones, J. Dorfman for Impα3, and T. Stukenberg, R. Day, and X. Lu for helpful suggestions.

This work was supported by grant GM50526 from the NIH and NIH predoctoral Cell and Molecular Biology training grant T32 GM008136.

Submitted: 24 March 2008
Accepted: 11 August 2008

binding but allosterically inhibits association with histones. In its closed state, RCC1 has a low affinity for both DNA and histones. Binding of Ran causes the tail to undergo a conformational switch to an open state, exposing the histone-binding surface and enabling the tail to interact efficiently with DNA. This interaction is enhanced by α-N-methylation. Error bars represent ±SD.

References

Bilbao-Cortés, D., M. Hetzer, G. Längst, P.B. Becker, and I.W. Mattaj. 2002. Ran binds to chromatin by two distinct mechanisms. *Curr. Biol.* 12:1151–1156.

Bischoff, F.R., and H. Ponstingl. 1991. Catalysis of guanine nucleotide exchange on Ran by the mitotic regulator RCC1. *Nature.* 354:80–82.

Carazo-Salas, R.E., G. Guarguaglini, O.J. Gruss, A. Segref, E. Karsenti, and I.W. Mattaj. 1999. Generation of GTP-bound Ran by RCC1 is required for chromatin-induced mitotic spindle formation. *Nature.* 400:178–181.

Caudron, M., G. Bunt, P. Bastiaens, and E. Karsenti. 2005. Spatial coordination of spindle assembly by chromosome-mediated signaling gradients. *Science.* 309:1373–1376.

Chen, T., T.L. Muratore, C.E. Schaner-Tooley, J. Shabanowitz, D.F. Hunt, and I.G. Macara. 2007. N-terminal alpha-methylation of RCC1 is necessary for stable chromatin association and normal mitosis. *Nat. Cell Biol.* 9:596–603.

Dignani, J.D., R.M. Lebovitz, and R.G. Roeder. 1983. Accurate transcription initiation by RNA polymerase II in a soluble extract from isolated mammalian nuclei. *Nucleic Acids Res.* 11:1475–1489.

Gruss, O.J., and I. Vernos. 2004. The mechanism of spindle assembly: functions of Ran and its target TPX2. *J. Cell Biol.* 166:949–955.

Gruss, O.J., R.E. Carazo-Salas, C.A. Schatz, G. Guarguaglini, J. Kast, M. Wilm, N. Le Bot, I. Vernos, E. Karsenti, and I.W. Mattaj. 2001. Ran induces spindle assembly by reversing the inhibitory effect of importin alpha on TPX2 activity. *Cell.* 104:83–93.

Hood, F.E., and P.R. Clarke. 2007. RCC1 isoforms differ in their affinity for chromatin, molecular interactions and regulation by phosphorylation. *J. Cell Sci.* 120:3436–3445.

Hutchins, J.R., W.J. Moore, F.E. Hood, J.S. Wilson, P.D. Andrews, J.R. Swedlow, and P.R. Clarke. 2004. Phosphorylation regulates the dynamic interaction of RCC1 with chromosomes during mitosis. *Curr. Biol.* 14:1099–1104.

Kalab, P., R.T. Pu, and M. Dasso. 1999. The Ran GTPase regulates mitotic spindle assembly. *Curr. Biol.* 9:481–484.

Kalab, P., K. Weis, and R. Heald. 2002. Visualization of a Ran-GTP gradient in interphase and mitotic *Xenopus* egg extracts. *Science.* 295:2452–2456.

Kalab, P., A. Pralle, E.Y. Isacoff, R. Heald, and K. Weis. 2006. Analysis of a RanGTP-regulated gradient in mitotic somatic cells. *Nature.* 440:697–701.

Klebe, C., H. Prinz, A. Wittinghofer, and R.S. Goody. 1995. The kinetic mechanism of Ran–nucleotide exchange catalyzed by RCC1. *Biochemistry.* 34:12543–12552.

Li, H.Y., and Y. Zheng. 2004. Phosphorylation of RCC1 in mitosis is essential for producing a high RanGTP concentration on chromosomes and for spindle assembly in mammalian cells. *Genes Dev.* 18:512–527.

Li, H.Y., D. Wirtz, and Y. Zheng. 2003. A mechanism of coupling RCC1 mobility to RanGTP production on the chromatin in vivo. *J. Cell Biol.* 160:635–644.

Lutter, L.C. 1978. Kinetic analysis of deoxyribonuclease I cleavages in the nucleosome core: evidence for a DNA superhelix. *J. Mol. Biol.* 124:391–420.

Moore, W., C. Zhang, and P.R. Clarke. 2002. Targeting of RCC1 to chromosomes is required for proper mitotic spindle assembly in human cells. *Curr. Biol.* 12:1442–1447.

Nemergut, M.E., and I.G. Macara. 2000. Nuclear import of the Ran exchange factor, RCC1, is mediated by at least two distinct mechanisms. *J. Cell Biol.* 149:835–850.

Nemergut, M.E., C.A. Mizzen, T. Stukenberg, C.D. Allis, and I.G. Macara. 2001. Chromatin docking and exchange activity enhancement of RCC1 by histones H2A and H2B. *Science.* 292:1540–1543.

Nemergut, M.E., M.E. Lindsay, A.M. Brownawell, and I.G. Macara. 2002. Ran-binding protein 3 links Crm1 to the Ran guanine nucleotide exchange factor. *J. Biol. Chem.* 277:17385–17388.

Renault, L., N. Nassar, I. Vetter, J. Becker, C. Klebe, M. Roth, and A. Wittinghofer. 1998. The 1.7 A crystal structure of the regulator of chromosome condensation (RCC1) reveals a seven-bladed propeller. *Nature.* 392:97–101.

Renault, L., J. Kuhlmann, A. Henkel, and A. Wittinghofer. 2001. Structural basis for guanine nucleotide exchange on Ran by the regulator of chromosome condensation (RCC1). *Cell.* 105:245–255.

Sandeen, G., W.I. Wood, and G. Felsenfeld. 1980. The interaction of high mobility proteins HMG14 and 17 with nucleosomes. *Nucleic Acids Res.* 8:3757–3778.

Seino, H., N. Hisamoto, S. Uzawa, T. Sekiguchi, and T. Nishimoto. 1992. DNA-binding domain of RCC1 protein is not essential for coupling mitosis with DNA replication. *J. Cell Sci.* 102:393–400.

Silverman-Gavrila, R.V., and A. Wilde. 2006. Ran is required before metaphase for spindle assembly and chromosome alignment and after metaphase for chromosome segregation and spindle midbody organization. *Mol. Biol. Cell.* 17:2069–2080.

Simon, R.H., and G. Felsenfeld. 1979. A new procedure for purifying histone pairs H2A + H2B and H3 + H4 from chromatin using hydroxylapatite. *Nucleic Acids Res.* 6:689–696.

Talcott, B., and M.S. Moore. 2000. The nuclear import of RCC1 requires a specific nuclear localization sequence receptor, karyopherin alpha3/Qip. *J. Biol. Chem.* 275:10099–10104.

Terry, L.J., E.B. Shows, and S.R. Wente. 2007. Crossing the nuclear envelope: hierarchical regulation of nucleocytoplasmic transport. *Science.* 318:1412–1416.

Trinkle-Mulcahy, L., and A.I. Lamond. 2007. Toward a high-resolution view of nuclear dynamics. *Science.* 318:1402–1407.

Walther, T.C., P. Askjaer, M. Gentzel, A. Habermann, G. Griffiths, M. Wilm, I.W. Mattaj, and M. Hetzer. 2003. RanGTP mediates nuclear pore complex assembly. *Nature.* 424:689–694.

Yoon, S.O., S. Shin, Y. Liu, B.A. Ballif, M.S. Woo, S.P. Gygi, and J. Blenis. 2008. Ran-binding protein 3 phosphorylation links the Ras and PI3-kinase pathways to nucleocytoplasmic transport. *Mol. Cell.* 29:362–375.

Zhang, C., and P.R. Clarke. 2000. Chromatin-independent nuclear envelope assembly induced by Ran GTPase in *Xenopus* egg extracts. *Science.* 288:1429–1432.

Zhang, C., M. Hughes, and P.R. Clarke. 1999. Ran-GTP stabilises microtubule asters and inhibits nuclear assembly in *Xenopus* egg extracts. *J. Cell Sci.* 112:2453–2461.